RL-TR-92-242
In-House Report
October 1992

P+ CONTACTS ON GaAs FOR SEMICONDUCTOR LASERS

Michael A. Parker, Alexander Olewicz, Stuart I. Libby,
David A. Honey, Major, USAF,
OCPB; Paul D. Swanson; Cornell University

APPROVED FOR PUBLIC RELEASE; DISTRIBUTION UNLIMITED.

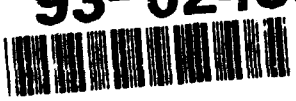

Rome Laboratory
Air Force Materiel Command
Griffiss Air Force Base, New York

This report has been reviewed by the Rome Laboratory Public Affairs Office (PA) and is releasable to the National Technical Information Service (NTIS). At NTIS it will be releasable to the general public, including foreign nations.

RL-TM-92-242 has been reviewed and is approved for publication.

APPROVED: 

JAMES W. CUSACK, Chief
Photonics & Optics Division

FOR THE COMMANDER: 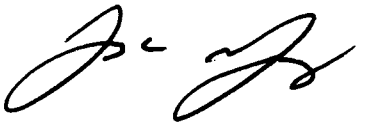

JAMES W. YOUNGBERG, LtCol, USAF
Deputy Director
Surveillance and Photonics Directorate

If your address has changed or if you wish to be removed from the Rome Laboratory mailing list, or if the addressee is no longer employed by your organization, please notify RL (OCPB) Griffiss AFB NY 13441-5700. This will assist us in maintaining a current mailing list.

Do not return copies of this report unless contractual obligations or notices on a specific document require that it be returned.

REPORT DOCUMENTATION PAGE

Form Approved
OMB No. 0704-0188

1. AGENCY USE ONLY (Leave Blank)	2. REPORT DATE	3. REPORT TYPE AND DATES COVERED
	October 1992	In-House Jun 90 - Feb 92

4. TITLE AND SUBTITLE
P+ CONTACTS ON GaAs FOR SEMICONDUCTOR LASERS

5. FUNDING NUMBERS
PE - 62702F
PR - 4600
TA - P3
WU - 05

6. AUTHOR(S)
M. A. Parker, A. Olewicz, S. I. Libby, D. A. Honey, Major, USAF, P. D. Swanson

7. PERFORMING ORGANIZATION NAME(S) AND ADDRESS(ES)
Rome Laboratory (OCPB)
26 Electronic Parkway
Griffiss AFB NY 13441-4515

Cornell University
Dept of Elec Engr
212 Phillips Hall
Ithaca NY 14853

8. PERFORMING ORGANIZATION REPORT NUMBER
RL-TR-92-242

9. SPONSORING/MONITORING AGENCY NAME(S) AND ADDRESS(ES)
Rome Laboratory (OCPB)
26 Electronic Parkway
Griffiss AFB NY 13441-4515

10. SPONSORING/MONITORING AGENCY REPORT NUMBER

11. SUPPLEMENTARY NOTES
Rome Laboratory Project Engineer: Michael A. Parker/OCPB (315) 330-7671

12a. DISTRIBUTION/AVAILABILITY STATEMENT
Approved for public release; distribution unlimited.

12b. DISTRIBUTION CODE

13. ABSTRACT (Maximum 200 words)
Discusses the physics and engineering of semiconductor electrical contacts and the importance of low resistance Ohmic contacts for the best performance from electronic devices. A simple method is used to deduce the resistance of the electrical contacts and the bulk semiconductor. The fabrication process for P+ GaAs contacts is discussed. Test results are presented for the resistance of the metal electrodes, P+ GaAs bulk, the intrinsic contact resistance and the temperature dependence of the metal and P+ GaAs. The distributed impedance of the contact structure for semiconductor lasers is discussed.

14. SUBJECT TERMS
electrical contacts, GaAs, distributed impedance, lasers

15. NUMBER OF PAGES
24

16. PRICE CODE

17. SECURITY CLASSIFICATION OF REPORT	18. SECURITY CLASSIFICATION OF THIS PAGE	19. SECURITY CLASSIFICATION OF ABSTRACT	20. LIMITATION OF ABSTRACT
UNCLASSIFIED	UNCLASSIFIED	UNCLASSIFIED	U/L

ACKNOWLEDGEMENTS

The authors wish to acknowledge useful discussions with W. Grande at Kodak in Rochester N.Y., the personnel at the National Nanofabrication Facility and Dr. C. L. Tang's Group at Cornell University and with other individuals in the Digital Photonics Branch at Rome Laboratory.

A. Olewicz and S. Libby assisted with the measurements to determine the temperature dependence of the resistance of the contact structures, D. Honey assisted with the photolithography, P. D. Swanson provided useful discussions on the zinc diffusion process.

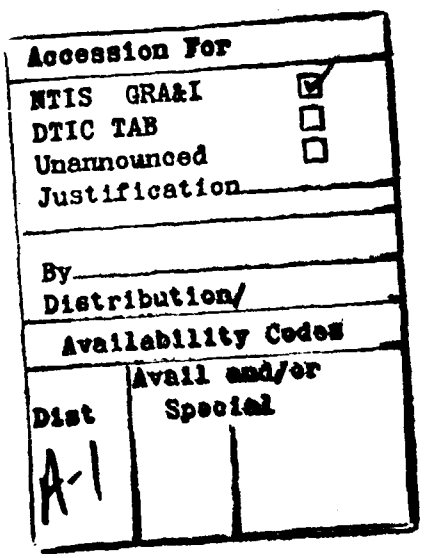

TABLE OF CONTENTS

INTRODUCTION

Electrical contacts have been studied since the middle of the last century.[1-2] Since the late 1940's, industry has utilized the properties of electrical contacts to realize semiconductor components such as high speed Schottky diodes and integrated electro-optic circuits. Electrical contacts are the most basic and, at the same time, one of the most important parts of modern integrated circuitry.

Electronic and electro-optic devices, which do not require the diode properties of a metal-semiconductor interface, are usually given Ohmic, low resistance electrical contacts; without this type of contact, the performance of the device would be linked to the properties of the contact itself. Ohmic electrical contacts have linear current-voltage (I-V) characteristics by definition; this permits the device characteristics to be observed independently of the contact characteristics. The contacts should generally have low intrinsic resistance to improve the performance of the device. Specifically, lowered contact resistance increases the device bandwidth and decreases both the noise figure and the power dissipation. Under the appropriate conditions, a device with Ohmic contacts can still have a transient response which is dominated by the depletion or accumulation region at the metal-semiconductor interface.[3-6]

The Ohmic properties of the contact are a result of thermionic field emission at the metal - semiconductor interface.[2] Thermionic field emission occurs at the metal - semiconductor interface for narrow or small energy barriers presented by bent conduction or valence bands; the width of these barriers can be controlled with high levels of doping. Generally, the conditions of the surface of a semiconductor determine the shape of the conduction and valence bands near the surface. Surface states can *pin* the Fermi energy level in the semiconductor to a given value. In this case, the width and height of the barrier is determined by the relative magnitudes of the density of states at the surface and the density of donor or acceptor states in the bulk. Metal evaporated onto a surface with a high number of surface states will have little affect on the band bending. However, the width and height of the barrier in a semiconductor with few surface states is directly related to the work function of the metal evaporated onto the surface. The width of the barrier can be reduced to enhance tunnelling (field emission) by heavily doping the semiconductor near the surface. Carriers can surmount the barriers (thermionic emission) or tunnel through narrow parts of it at higher energies by absorbing phonons from the lattice. Generally, field emission is used to provide Ohmic contacts but thermionic emission has been used in recent heterostructure materials where the band discontinuities at the interfaces have been lowered by band gap engineering.[7]

Semiconductor devices such as PIN photodiodes, transistors and lasers, have diode-like structures and therefore use both N^- and P^+ Ohmic contacts. The type of contact determines the processing steps and

the type and number of metals evaporated onto the wafer. The high doping levels can be achieved in several ways. The dopants can be placed into the substrate during an MBE growth phase, they can be diffused into the substrate in a high temperature oven or they can be included as a layer of metal and then diffused into the substrate during a subsequent alloying step. The P^+ contacts on GaAs discussed in this technical memorandum use the second method with zinc as the dopant. Consideration must be given to the adhesive properties between the metal and the substrate. Some metals such as titanium or chrome adhere better than others and are therefore evaporated onto the substrate first. The first layer of metal on GaAs for P^+ contacts consists of titanium; chrome should not used for this purpose with GaAs since it produces deep traps. The second layer consists of platinum which provides a diffusion barrier between a top gold layer and the GaAs wafer. An N^- contact has a top layer of gold to getter the Ga out of the substrate so that Ge from one of the metal layers can substitute at the resulting vacant lattice sites in the GaAs to serve as a dopant. The gold layer on the P^+ contacts provides a highly conductive layer so that the metal will have the lowest possible resistance and be immune to corrosion. After the metals have been evaporated onto the surface, the wafer is alloyed to diffuse any metal dopants into the substrate and to activate those dopants.

The remainder of this technical memorandum discusses the basic circuit model for the contact, the fabrication process, the experimental data and the author's interpretation of the data. An appendix contains a distributed impedance model for the effective resistance of an electrode structure similar to that used for semiconductor lasers.

BASIC CIRCUIT MODEL

The simplest model defines a contact resistance R_c and bulk GaAs resistance R_b.[1] The contact resistance occurs at the MS interface as a result of the energy barrier there. The resistance of a metal electrode R_m becomes important when it is comparable in value with the resistance of the bulk semiconductor. As is well known, Schottky barriers have both resistive and reactive components; thus, for the general case, the response of the electrical contact depends on the frequency content of the drive signal. For low frequency work, the reactive component of the contact is negligible. The inset to figure 1 shows the low frequency model.

The values of the contact and bulk resistance can be determined by use of an appropriate test structure. One of the simplest geometries consist of a series of metal electrodes evaporated onto the GaAs. In one case, the electrodes are placed at regular intervals along the length of the GaAs wafer. In another case, the distance separating two adjacent electrodes D_i changes along the length of the wafer. For either case, assuming that the contacts are uniformly fabricated across the surface of the sample, the plot of the total resistance R as a function of the separation distance D is a straight line. The total resistance between the pads is defined by

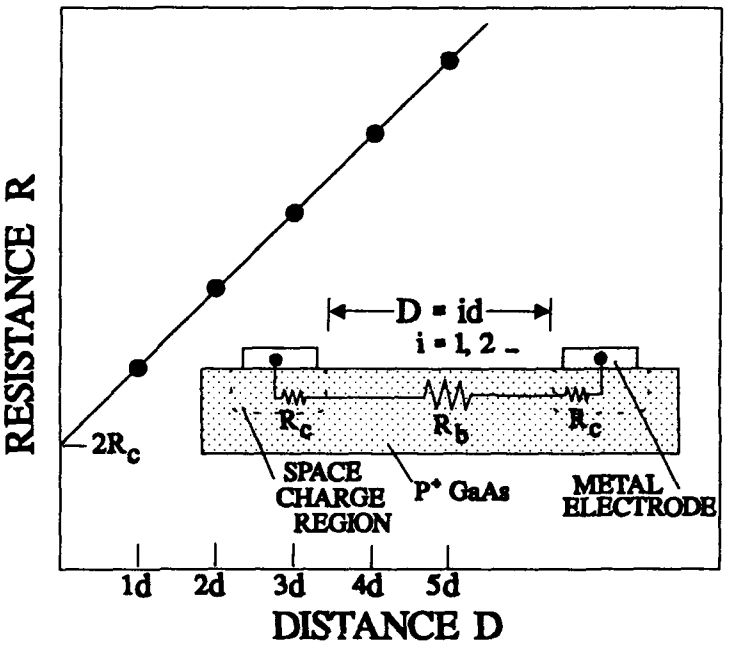

Figure 1: The expected plot of resistance between two metal electrodes as a function of separation between the pads. The intercept of the straight line with the resistance axis yields $2R_c$ and the slope of the line yields the bulk resistance. The inset shows the low frequency model. The electrodes are spaced by D=id where *i* is an integer.

$$(1) \qquad R = 2R_c + \frac{D}{d} R_b$$

where *D* is the distance separating two adjacent electrodes, *d* is the smallest such distance for a given contact geometry and R_b is the bulk resistance corresponding to the distance *d*. The intercept of the line with the resistance axis is $2R_c$ and the slope is R_b/d. The space charge region can give rise to photocurrents when illuminated which can be modelled by a current source in parallel with the contact impedance. In addition, the GaAs can exhibit a photoconductive response. Photocurrents originating in the space charge region produce a non-linearity in the I-V curves at low applied voltages if they are not specifically taken into account. The photoconductive response changes the slope of the I-V curves. The experiments reported here were performed in the dark and the photocurrents were determined to be negligible.

The electrical contact can be represented accurately as a transmission line.[1] Such an approach models the resistance and capacitance as a distributed impedance. Generally, the metallization is assumed to have negligible resistance for the calculations. A distributed impedance model can also be used to

explain results obtained from certain electrode geometries as discussed in the appendix. Single mode semiconductor lasers generally have long, narrow electrodes on one side of the wafer and a large area, low resistance electrode on the other side which carries the current common to all of the devices on the wafer. The narrow electrodes can have resistances on the same order of magnitude as the laser. The voltage drop along these narrow electrodes can be significant at high currents and, as demonstrated in the appendix, this voltage drop is nonlinear with distance along the electrode. Such a voltage drop would result in uneven pumping of a laser cavity. Thus, the distributed impedance of the contact, the metal and the semiconductor are important to the operation of semiconductor lasers, laser amplifiers and laser based optical logic gates.

FABRICATION

The contacts were fabricated on an n-type GaAs wafer so that each P^+ doped region, a resistive element, can be positioned in the potential well of a reversed biased diode. During the test phase, the current flow is confined to a narrow channel between the pads by reverse biasing the contact structure with respect to the substrate. However, with sufficiently high doping levels, leakage current from the doped region to the substrate is generally negligible. The following outlines the fabrication process used to produce the contact structures for this study.

(1) The wafer surfaces were cleaned with a camel hair brush and liquid Ivory dish soap and rinsed in DI water. The wafer was dipped in Acetone, Methonal, Isoproponal and DI water to remove grease and residues from the surface. A solution of Ammonium Hydroxide and DI water, in the ratio of 1:15, was used to remove organics from the surface and to perform a slight etch on the surface oxides.

(2) A 1500 angstrom thick layer of SiO_2 was deposited over the wafer surface in a Plasma Enhanced Chemical Vapor Deposition (PECVD) system at 250 ^oC to provide (i) a diffusion mask for the subsequent processing step and (ii) electrical isolation for the finished device. The glass layer was patterned in a Reactive Ion Etcher (RIE) with CHF_3 gas; the mask for this process consisted of a patterned Shipley 1400-27 photoresist layer. After patterning the SiO_2 layer, an oxygen plasma was used to remove the remaining photoresist.

(3) Regions of the n-type GaAs, as defined by the openings in the SiO_2, were doped p-type by a Zinc diffusion process. The Zinc was diffused to a depth of 0.7 μm during a 1/2 hour bake at 650 ^oC in a diffusion oven.

(4) The metal electrodes were defined by photolithography. The metal was evaporated in an electron beam evaporator and then a lift off process produced the desired electrode pattern. A standard photoresist lift off process was unsuitable for use with the available electron beam evaporator. Heat transferred from the evaporated metal to the photoresist would have hardened the photoresist and made it difficult to remove. Instead, a One Step Two Level Etch process was used.[8] Layers of polyimide and SiO_2 were deposited across the surface. The first layer, polyimide, was spun on at 5K RPM, baked at 80 ^oC for 30 minutes and then baked at 150 ^oC for an additional 30 minutes as per the manufacturer's specifications. Next, a glass layer was deposited to a thickness of 800 angstroms in the PECVD system at a temperature of 150 ^oC; the lower deposition temperature prevented the polyimide from becoming impervious to solvants. A patterned photoresist layer was used as an etch mask for the glass which was etched in CHF_3 in the RIE. The patterned glass layer served as the etch mask for the polyimide. An oxygen plasma etched the polyimide and the remaining photoresist. After the metal was evaporated across the wafer surface, the wafer was dipped into methylene chloride which caused the polyimide to lift off both the glass and the unwanted metal.

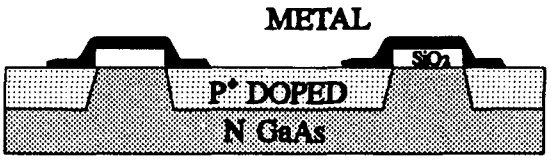

Figure 2: The layered structure of the electrodes.

(5) The metal layer consisted of three metals. A 1500 angstrom Au layer was deposited on top of a 200 angstrom Pt layer which was on top of a 200 angstrom layer of Ti. Later, the metal contacts were alloyed at 360 ^oC for 3 minutes in a hydrogen atmosphere. The basic electrode structure appears in figure 2.

The geometry of the contacts appears in figure 3. The nomenclature is as follows. The resistive element between the pads is either Metal *M* or P^+ GaAs *G*. The length of the resistive elements is either fixed or Variable *V* across the wafer. In the case of a fixed length, the last several digits in the structure name represents the distance in microns. In the variable cases, the last two digits give the minimum separation in microns. The column D_i gives the length of the resistive elements in units of microns for each integer i. The figure contains the dimensions of the pads and the amount of overlap of the pad and the GaAs resistive elements.

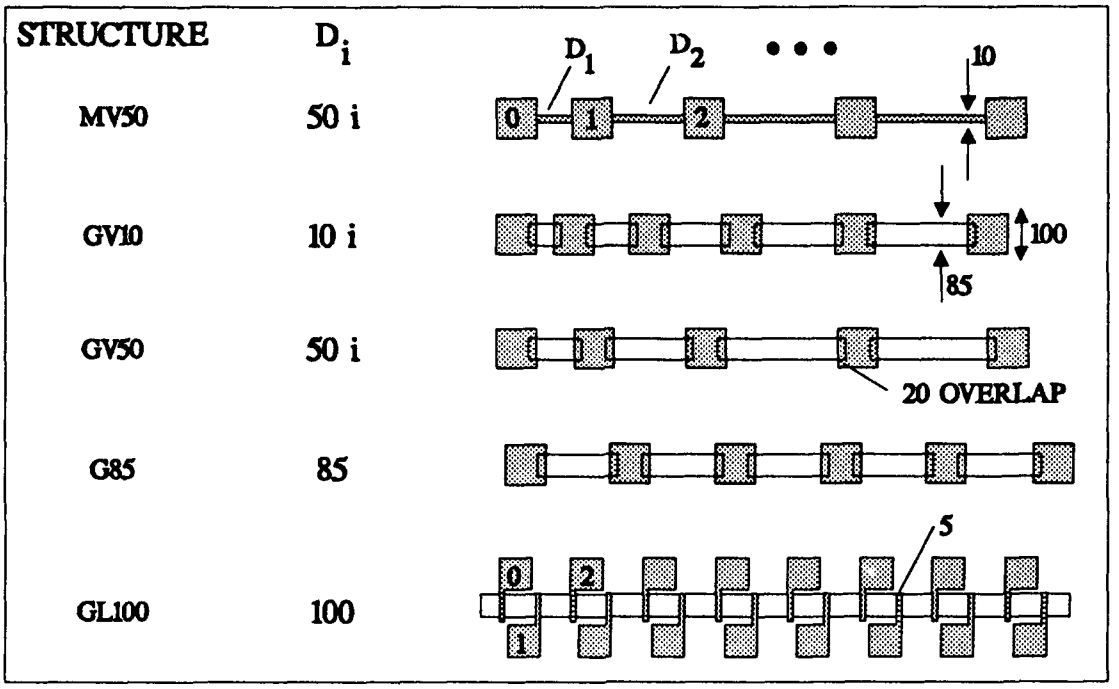

Figure 3: The geometry of the contacts fabricated to determine contact resistance. The distances D_i are in mircons where *i* is an integer. The top set, MV50, has metal for the resistive element and a variable distance separating the pads. The remaining sets have P^+ GaAs as the resistive elements between the pads. The bottom set is the laser-like structure discussed in the text in conjuction with distributed impedance.

EXPERIMENTAL

The resistances were determined with Keithley digital multimeters by measuring both the voltage applied to the contact structure and the resulting current; for low current levels, a low noise current amplifier was added to the experimental setup. The I-V curves were determined for 6 decades of current with this arrangement. Tungsten and copper probe tips were used to provide the bias to the pads. The copper probes were made from solid telephone wire with the tips polished to diameters on the order of 10 μm. The resistance of the probe tips was determined to be 0.178 Ω/tip by placing both tips close together on a single large metal pad and then measuring the I-V characteristics. The setup appears in the inset to figure 4.

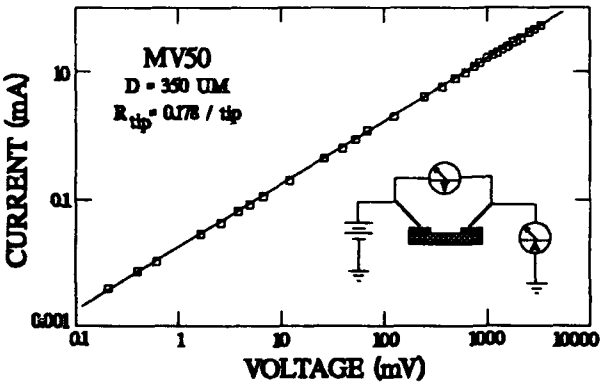

Figure 4: Typical plot of current versus voltage for the contact structures. The above graph has the characteristics for the MV50 structure. The probe resistance of 0.356 Ω has not been factored out of the data.

Measurements were made of (1) the I - V characteristics, (2) the resistance as a function of the distance between the pads for a constant current and (3) the temperature dependence of the resistance for metal and the doped GaAs. Typical I-V and R-D plots appear in figures 4 and 5. For the R-D plots, the current was held constant. The R-D plots generally become nonlinear for large separation distances due to variations in processing across the surface of the wafer. Measurements were made on the GL100 contact structure to determine the ratio $\Delta V/V_0$, the ratio of the voltage drop along the 85 μm length of metal versus the voltage applied to the two electrodes. Both alloyed and unalloyed contact structures were tested. The tests indicated that (1) the metal had a ratio of resistivity to thickness of $\rho / T = 1.6\ \Omega / \square$ independent of the alloying, (2) the G85 style contacts had a resistance $R_c = 1\ \Omega$ (or 4 Ω/□) after alloying and a negative value before alloying, and (3) the GL100 contacts had a resistance of 8 Ω (or 120 Ω/□), independent of alloying, and values for $\Delta V / V_0$ of 17% and 10% for type 1 structures with an electrode separation distance of $D_1 = 100$ μm and type 2 structures with an electrode separation distance of $D_1+D_2 = 200$ μm, respectively. Tests on the G85 style contacts further indicated a value of 29 Ω/□ for the bulk P^+ material. In all cases, the contacts were found to be Ohmic in the range of 1 μA to 50 mA. The metal resistance was expected to drop by about an order of magnitude after alloying but it did not do so.

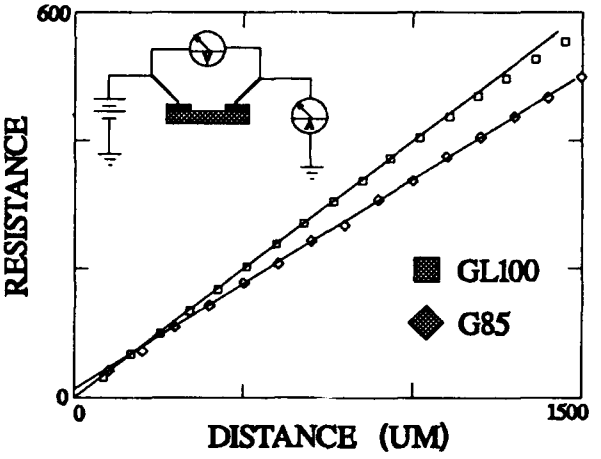

Figure 5: Typical plots of resistance vs. distance for the G85 and GL100 contact structures. The current was maintained at 5 mA.

Table 1 contains a summary of the resistances obtained from the contact structures. The ratio ρ / T is generally in the range of 30 for the doped GaAs. The contact resistance depends on the amount of overlap between the metal pad and the GaAs. Note the large value of the contact resistance for the GL100 structure. Most of this resistance is attributable to the resistance of the metal in the narrow metal electrode. The effective resistance R_{eff} is related to the contact and bulk resistance by $R_{eff} = 2R_c + R_b$. The GL100 structure has two values for R_{eff} which correspond to two different distances separating the pads. The larger distance corresponds to the situation where an electrode lies between the two current carrying electrodes.

TABLE OF RESISTANCES

TYPE	R_b	R_c	R_{eff}
MV50	1.6 Ω/❑	0	
GV10	3.16 26.7 Ω/❑	3.2 13.6 Ω/❑	9.56
GV50	20.1 34.1 Ω/❑	–0.9	
G85	29.0 29 Ω/❑	1 4 Ω/❑	31
GL100	32.2 27.4 Ω/❑	8 120 Ω/❑	50 / 100μ 81.5 / 200μ

TABLE 1: Summary of resistances obtained from the R-D graphs. The bulk resistance R_b and contact resistance R_c are listed in Ohms and as the ratio of resistivity to thickness, ρ/T. The bulk resistance in Ohms refers to the resistance of the GaAs for the minimum separation between the electrodes. GL100 has two values for R_{eff} corresponding to pad separations of 100 and 200 μm.

The resistance of metals and highly doped semiconductors increase with temperature. For these materials, there are several contributions to the resistance which includes electron and hole scattering from lattice defects and phonons. Phonon scattering is the most important mechanism for the temperature dependence of the resistivity. As temperature increases, the number of phonons increases and, therefore, the mean free path of the electrons and holes decreases. As a result, the resistance of metals and highly doped semiconductors increase with temperature. This contrasts with intrinsic semiconductors where the resistivity decreases with temperature as predicted by the temperature dependence of the Fermi function.

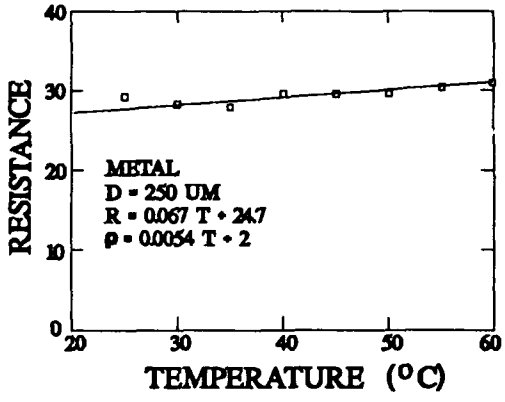

Figure 6: Temperature dependence of the resistance for the metal used in the contact structures. The length of the metal was 250 μm and the cross section area was 2 x 10 μm^2. The resistivity ρ has units of Ω–μm.

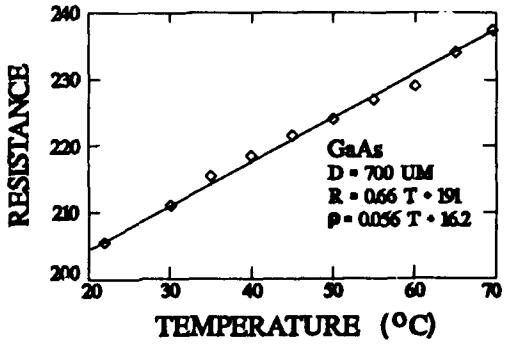

Figure 7: Temperature dependence of the resistance for the P^+ GaAs used in the contact structures. The length of the GaAs was 700 μm and the cross section area was 0.7 x 85 μm^2. The resistivity ρ has units of Ω–μm.

The metal or P^+ GaAs can be used to sense the junction temperature of semiconductor lasers. For this reason, the variation of the metal and P^+ GaAs resistance with temperature was determined. The wafer with the contact structures was mounted on a hot plate to provide control over the temperture of the wafer. Figures 6 and 7 show the results. Over a range of approximately 40 °C, the resistance of the metal varied by several Ohms while that for the P^+ GaAs varied by approximately 30 Ω. The inset to the graphs

contain the temperature dependence of the resistivity ρ in units of Ω–μm as calculated from the resistance and sample size. The calculation for the resistivity of the P^+ GaAs used the zinc diffusion depth of 0.7 μm for the thickness.

DISCUSSION

The Table of Resistances contains several anomalies. The experimentally determined resistance of the metal is an order of magnitude larger than the value calculated from the thickness and conductivity of the layers. The contact resistance of the GV85 style contacts changed from negative to positive values after alloying. The contact resistance was high for the GL100 style. The experimental values of $\Delta V/V_0$ differ by 15% from those predicted by the distributed impedance models discussed in the appendix.

The anamalies can be explained as follows. The discrepancy between the observed and predicted values of the metal resistivity might be partially attributed to thin film effects and to the fact that probes tend to destroy the electrical pads during testing. The change from negative to positive values for the contact resistance for the G85 style contacts upon alloying can be attributed to changes in the stochiometry and structure of the metal-semiconductor interface. The experimentally determined values for the contact resistance are quite sensitive to any curvature in the R-D curves which might account for the negative values reported for the contact resistance of the GV50 style. The high resistance for the GL100 contacts is due to the combination of two facts: (1) the extrapolation procedure extracts R_c and R_b as if the total distributed impedance could be written as $2R_c + R_b$ instead of the nonlinear expressions obtained in the appendix; (2) the large value obatined for the resistance of the metal ($\rho/T = 1.6\ \Omega/\square$).

The distributed impedance model discussed in the appendix provides some insight into the behavior of the GL100 electrode structure. The set consists of two basic types as shown in figure A1. Adjacent electrodes in the GL100 set are type 1. Two electrodes in the set which are separated by a third electrode are the type 2. Electrodes must be modelled as distributed impedances when the resistance of the metal electrodes is close to that of the semiconductor. For the GL100 set, the resistance of the metal electrode along the direction of current flow is calculated from table 2 to be $R_m = 27\ \Omega$. The G85 value for R_b, for example, yields the value $R_g = 34\ \Omega$ for the resistance of 100 μm of the GaAs. The model predicts $\Delta V/V_0$ to be 26% and 15% for 100 and 200 μm respectively. These values disagree with the experimental values by about 15% in both cases.

The discrepancy between the experimental and calculated values of $\Delta V/V_0$ can be attributed to several sources including a variation in the processing parameters across the wafer surface and, in particular, to the deviation of the actual path of current flow in the structure from that assumed in the model. The

model assumes that the current flows in a straight line perpendicular to the metal electrodes. For the type 1 structure, for example, the actual path will be diagonal across the wafer if the potential difference for a diagonal path adequately compensates for the increased resistance along that path. The difference in values can be partially attributed to the fact that the metal electrodes have slightly larger resistances than the quoted 27 Ω due to an additional 10 to 20 μm of metal added to the electrode for placement of the probes.

The values in table 1 can be used to arrive at an approximate doping level for the P^+ material. Given that the doping extends to a depth of T = 0.7 μm, plots of resistivity versus doping, such as in Sze's book[9] yield, a doping level on the order of 10^{19}. This number is consistent with other measurements made in the lab.

SUMMARY AND CONCLUSIONS

This technical memorandum has briefly discussed the physics of semiconductor electrical contacts and the importance of low resistance Ohmic contacts for proper device performance. A simple method was presented for deducing the resistance of the electrical contacts and the bulk GaAs semiconductor. The fabrication of several contact structures was discussed. The structures were tested for the resistance of the metal and P^+ GaAs, the contact resistance and the temperature dependence of the resistance of the metal and P^+ GaAs. The appendix to this technical memorandum discusses the distributed resistance of the GL100 contact structure.

The contact study has important implications for laser-based logic gates, optical amplifiers and electrically pumped optical waveguides which use similar contact structures. Current injected into these devices will not evenly distribute along the contact length due to the high distributed impedance. For the laser-based logic gates, the interaction between adjacent lasers will depend on the relative positions of the two devices in the integrated circuit. The gain of the laser amplifier which employs these contacts will be largest near the end where the current is injected. It is possible for the gain to vary in such a way that the amplifier or laser is both above and below transparency or threshold along the length of the device.

APPENDIX: DISTRIBUTED IMPEDANCE MODELS

A distributed impedance approach can also be used to explain results obtained from certain electrode geometries. The electrodes shown in figure A1 approximate a set of contacts fabricated for this study. Semiconductor lasers use a similar construction except one of the metal electrodes would be a very low resistance one which carries the current common to all of the devices on the wafer. The narrow metal electrodes have resistances on the same order of magnitude as the doped GaAs. The voltage drop along the metal electrodes becomes significant at high currents; this drop is nonlinear with the distance along the electrodes.

The electrode structures shown in figure A1 can be analyzed by dividing the metal electrodes and GaAs into lengths dx. The structures are then represented as the series combination of resistances dR_m for the electrodes and the parallel combination of conductances dG for the semiconductor. The voltages $V_t(x)$ and $V_b(x)$ refer to the voltage of the node at point x on the upper and lower branches respectively. The current $I_t(x)$ and $I_b(x)$ are calculated by applying Ohm's law to each element dR_m with dV_t and dV_b as the voltage drop between adjacent nodes.

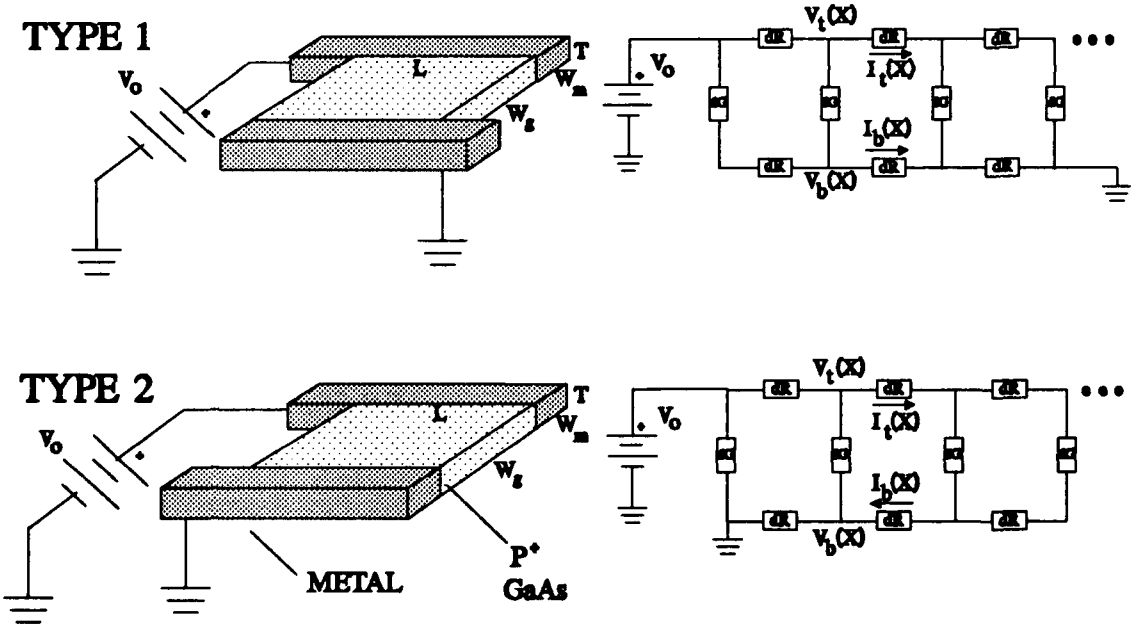

Figure A1: Two contact structures (left) and the corresponding discrete component circuit models (right). The top and bottom circuit elements dR represent the infinitesimal resistances along the metal pads. dG is the conductance of a thin strip of GaAs between the two pads. The contact resistance R_c is included with the dG term.

The basic relation between resistance R, resistivity ρ, length L and cross sectional area A, namely $R = \rho \frac{L}{A}$, can be applied to the metal electrodes as $dR_m = \rho_m \frac{dx}{A} = R_m \frac{dx}{L}$ and to the GaAs as $dG = \frac{T\,dx}{\rho_g W_g} = \frac{1}{R_g}\frac{dx}{L}$. The circuit equations and boundary conditions for the type 1 and 2 electrode structures are:

Type 1 Equations

(A1a) $dV_t = - I_t(x)\, dR_m$
(A2a) $dV_h = - I_h(x)\, dR_m$
(A3a) $dI_t = - dG\, [V_t(x) - V_h(x)]$
(A4a) $\frac{dI_t}{dx} = \frac{dI_b}{dx}$
(A5a) $V_o - V_t(x) = V_h(L-x)$

Type 2 Equations

(A1b) $dV_t = - I_t(x)\, dR_m$
(A2b) $dV_h = I_h(x)\, dR_m$
(A3b) $dI_t = - dG\, [V_t(x) - V_h(x)]$
(A4b) $I_t(x) = I_h(x)$
(A5b) $V_o - V_t(x) = V_h(x)$

Type 1 Boundary Conditions

(A6a) $V_t(0) = V_o$
(A7a) $V_h(L) = 0$
(A8a) $I_t(L) = 0$
(A9a) $V_h(0) = 0$

Type 2 Boundary Conditions

(A6b) $V_t(0) = V_o$
(A7b) $V_h(0) = 0$
(A8b) $I_t(L) = 0$
(A9b) $I_h(L) = 0$

The circuit equations can be rewritten as first order, linear differential equations in *x* as

Type 1 Equations

(A10a) $\frac{dV_t}{dx} = -I_t \frac{R_m}{L}$
(A11a) $\frac{dV_b}{dx} = - I_b \frac{R_m}{L}$
(A12a) $\frac{dI_t}{dx} = - \frac{1}{LR_g} [V_t(x) - V_b(x)]$
(A13a) $\frac{dI_b}{dx} = - \frac{dI_t}{dx}$
(A14a) $V_o - V_t(x) = V_h(L-x)$

Type 2 Equations

(A10b) $\frac{dV_t}{dx} = -I_t \frac{R_m}{L}$
(A11b) $\frac{dV_b}{dx} = I_b \frac{R_m}{L}$
(A12b) $\frac{dI_t}{dx} = - \frac{1}{LR_g} [V_t(x) - V_b(x)]$
(A13b) $I_h(x) = I_t(x)$
(A14b) $V_o - V_t(x) = V_h(x)$

Equations A3 and A12 are obtained from the current flow from the upper to the lower branch. Equations A4, A5, A13 and A14 are obtained from the symmetry of the circuits.

Solutions to Type 1 Equations:

$$(A15)\quad \frac{V_t(x)}{V_o} = \frac{e^{b(1-x/L)} + e^{bx/L} + \frac{b}{L}(1 - e^b)\, x + 1 - b + (1 + b)\, e^b}{2\,(1 + e^b) - b\,(1 - e^b)}$$

$$(A16)\quad \frac{V_b(x)}{V_o} = \frac{-e^{b(1-x/L)} - e^{bx/L} + \frac{b}{L}(1 - e^b)\, x + 1 - b + (1 + b)\, e^b}{2\,(1 + e^b) - b\,(1 - e^b)}$$

$$(A17)\quad \frac{I_t(x)}{V_o/R_m} = \frac{b\, e^{b(1-x/L)} - b\, e^{bx/L} - b\,(1 - e^b)}{2\,(1 + e^b) - b\,(1 - e^b)}$$

$$(A18)\quad \frac{I_b(x)}{V_o/R_m} = \frac{-b\, e^{b(1-x/L)} + b\, e^{bx/L} - b\,(1 - e^b)}{2\,(1 + e^b) - b\,(1 - e^b)}$$

where

$$(A19)\quad b = +\sqrt{\frac{2\,R_m}{R_g}}$$

Solutions to Type 2 Equations:

$$(A20)\quad V_t(x) = \frac{V_o}{2}\left(1 + \frac{e^{b(1 - x/L)} + e^{-b(1 - x/L)}}{e^b + e^{-b}}\right)$$

$$(A21)\quad V_b(x) = \frac{V_o}{2}\left(1 - \frac{e^{b(1 - x/L)} + e^{-b(1 - x/L)}}{e^b + e^{-b}}\right)$$

$$(A22)\quad I_t(x) = I_b(x) = \frac{V_o}{2}\sqrt{\frac{2}{R_m R_g}}\,\frac{e^{b(1 - x/L)} - e^{-b(1 - x/L)}}{e^b + e^{-b}}$$

where *b* is given by equation A19. Figure A2 shows $V_t(x)$ and $I_t(x)$ for the two types.

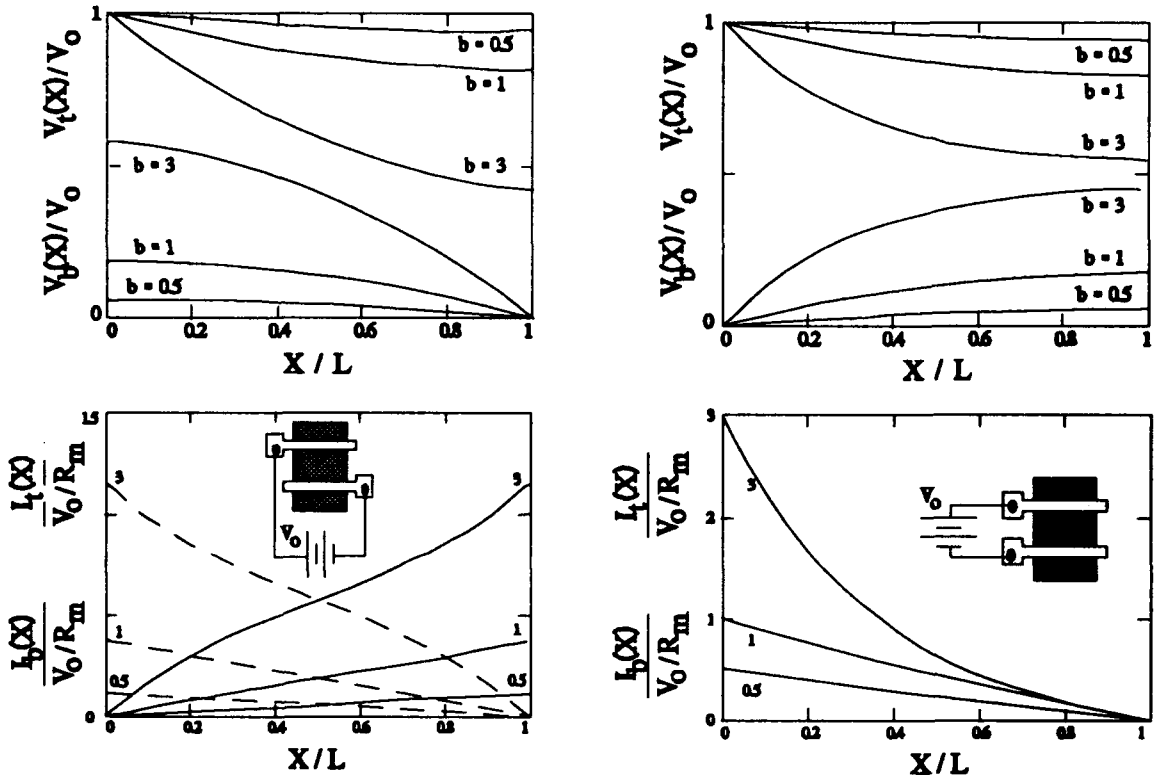

Figure A2: The voltage distribution (top) and current distribution (bottom) along the metal electrodes for the type 1 (left) and type 2 (right) electrode structures. The curves are parameterized by *b*. For the voltage plots, $V_t(x)$ and $V_b(x)$ are the top most and bottom most curves, respectively. The plots of the current in the top electrode for the type 1 structure (bottom left) are represented by dashed lines. Only one set of curves appears for the current in the electrodes of the type 2 structure since $I_t(x)$ and $I_b(x)$ are identical.

These two sets of solutions yield equivalent input resistances R_{eff} for the respective contact structure. R_{eff} is nonlinear in the GaAs and metal resistances and it is defined to be V_o / $I_t(0)$. Another quantity of interest is the ratio of the voltage drop along one of the narrow metal electrodes $\Delta V = V_o - V(L)$ to the voltage applied across the contact structure V_o. The two sets of equations yield the following results. A plot of the effective resistance appears in figure A3.

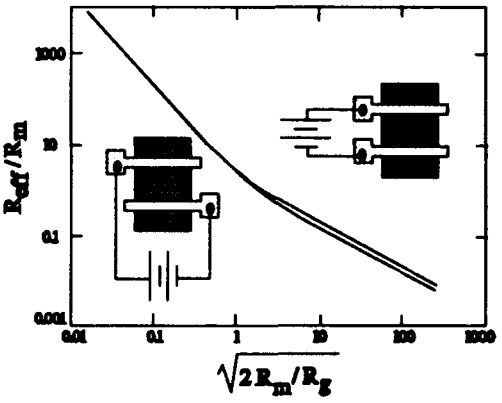

Figure A3: The effective input resistance as a function of the metal and P^+ GaAs resistance. The top and bottom curves correspond to the type 1 and type 2 structures respectively.

Type 1:

(A23a) $$R_{eff} = \sqrt{\frac{R_m R_g}{2}} \left(\frac{e^b + 1}{e^b - 1} + \frac{1}{2} \right)$$

(A24a) $$\frac{\Delta V}{V_0} = \frac{b\,(e^b - 1)}{2\,(1 + e^b) - b\,(1 - e^b)}$$

Type 2:

(A23b) $$R_{eff} = 2\sqrt{\frac{R_m R_g}{2}} \frac{e^b + e^{-b}}{e^b - e^{-b}}$$

(A24b) $$\frac{\Delta V}{V_0} = \frac{1}{2} - \frac{1}{e^b + e^{-b}}$$

The distributed impedance model for the GL100 contact structures can be summarized by figures A2 and A3. Figure A2 shows the voltage and current distribution along the length of the electrodes. As the ratio of the metal to GaAs resistance becomes small (small values for b), the voltage drop along the electrodes also becomes small. The upper right graph in figure A2 shows that the unconnected ends of the type 2 metal electrodes have voltages which can be close for large values of b. As expected from the zero current boundary conditions (Eqs. A8a and A8b), the current in each electrode approaches zero at one point along its length. Figure A3 shows that the geometry of the structure has little influence on its total resistance.

REFERENCES

1. R. E. Williams, Gallium Arsenide Processing Techniques, Artech House, Dedham (1984)
2. E. H. Rhoderick, Metal-Semiconductor Contacts, Clarendon Press, Oxford (1980)
3. M. A. Parker and E. A. Schiff, Appl. Phys. Lett. 48, 1087 (1986)
4. M. A. Parker, K. A. Conrad, E. A. Schiff, MRS Proceedings, Vol. 70 (1986)
5. R. A. Street, Phys. Rev. B, 32, 3910 (1985)
6. M. Abkowitz and H. Scher, Phil. Mag. 35, 1585 (1977)
7. G. R. Olbright, Photonic Technologies, Denver Co.
8. W. J. Grande, W. D. Braddcock, J. R. Shealy, C. L. Tang, Appl. Phys. Lett. 51, 2189 (1987)
9. S. M. Sze, Physics of Semiconductor Devices, 2nd Ed., John Wiley & Sons, New York (1981)

*U.S. GOVERNMENT PRINTING OFFICE: 1989-710-093-80110

MISSION

OF

ROME LABORATORY

Rome Laboratory plans and executes an interdisciplinary program in research, development, test, and technology transition in support of Air Force Command, Control, Communications and Intelligence (C^3I) activities for all Air Force platforms. It also executes selected acquisition programs in several areas of expertise. Technical and engineering support within areas of competence is provided to ESD Program Offices (POs) and other ESD elements to perform effective acquisition of C^3I systems. In addition, Rome Laboratory's technology supports other AFSC Product Divisions, the Air Force user community, and other DOD and non-DOD agencies. Rome Laboratory maintains technical competence and research programs in areas including, but not limited to, communications, command and control, battle management, intelligence information processing, computational sciences and software producibility, wide area surveillance/sensors, signal processing, solid state sciences, photonics, electromagnetic technology, superconductivity, and electronic reliability/maintainability and testability.